Electron Cyclotron Maser Emission from Power-Law Electron Distributions

Gregory D. Fleishman[1,2]

ABSTRACT

Electron cyclotron maser emission produced by superthermal electrons is known to be responsible for many kinds of astrophysical radio emission. The paper studies properties of this emission mechanism in the conditions typical for solar flares. Specifically, we assume broad (power-law) distributions of fast electrons over energy. The functional shape of the loss-cone pitch-angle distribution is specified based on recently obtained observational data. The dependences of the spatial growth rates of various wave-modes on the parameters of the fast electron distribution function (in particular, hardness and angular gradient) are studied in detail. Obtained properties of electron cyclotron maser emission are found to be pretty consistent with observed properties of solar radio spikes. Dependence of the growth rates on the plasma frequency to gyrofrequency ratio Y is analyzed for $Y = 0.1 - 2.5$. Important constraints for a particular harmonics dominating generation of solar radio spikes are found.

Subject headings: the Sun: flares, coherent emission—particle acceleration

1. Introduction

Electron cyclotron maser (ECM) emission is believed to be responsible for many kinds of solar, planetary and stellar radiation. While the idea of the direct amplification of the electromagnetic waves close to the gyrofrequency (and its harmonics) had been proposed long ago (Twiss 1958; Harris 1959; Schneider 1959; Sagdeev and Shafranov 1960), the understanding of its value for astrophysical applications appeared much later (Stepanov 1978; Wu and Lee 1979), when an important role of relativistic effects for ECM was discovered.

Since properties of ECM are sensitive to the details of electron distribution function, its direct quantitative application to a particular kind of astrophysical radio emission is not easy

[1]Purple Mountain Observatory, National Astronomical Observatories, Nanjing 210008, P.R. China

[2]Ioffe Institute for Physics and Technology, 194021 St.Petersburg, Russia

to perform. However, for a terrestrial Auroral Kilometric Radiation a detailed agreement between theory and observations was established (Wu 1985). Such a success was ensured by the use of the *measured* electron distribution function, plasma frequency and gyrofrequency for the respective calculations.

For the solar case, ECM models have been applied to interpret millisecond fine structures of decameter emission (Barrow et al. 1994), decimetric pulsations (Aschwanden and Benz 1988) and millisecond spikes (Holman et al. 1980; Melrose and Dulk 1982; Sharma and Vlahos 1984; Li 1986; Winglee et al. 1988; Aschwanden 1990; Fleishman 1994; Fleishman and Yastrebov 1994b; Ledenev 1998; Stupp 2000; Vlasov et al. 2002). However, for solar flares (as well as for other distant objects) such a detailed information about source parameters is unavailable, respectively, the identification of the emission mechanism is frequently less confident or less direct, at least.

There are strong evidences that narrowband millisecond spikes are indeed generated by ECM emission. It follows, e.g., from detailed comparison between the observed properties of solar radio spikes and predictions of various theoretical models (Fleishman and Melnikov 1998). Even stronger evidence is found recently from the analysis of correlations between the spikes and accompanying microwave continuum (Fleishman et al. 2003): they found, that spike-producing radio bursts reveal smaller plasma frequency to gyrofrequency ratios than other radio bursts, and the strongest averaged flux of the spike emission is observed when the fast electrons display the hardest energy spectra and the most anisotropic angular distribution.

The currently available data about the radio spikes are pretty consistent with the idea that the source of spike cluster is a loop filled by fast electrons and relatively tenuous background plasma. The trapped fast electrons have a power-law energy spectrum and a loss-cone angular distribution. Each single spike is generated in a local source inside this loop when the local anisotropy is increased compared with the averaged one to produce ECM emission.

The theory of ECM emission in the solar corona has been extensively developed for the recent years. Many papers (Sharma et al. 1982; Sharma and Vlahos 1984; Li 1986; Winglee and Dulk 1986; Aschwanden 1990; Fleishman and Yastrebov 1994a) (Fleishman and Yastrebov 1994c; Ledenev 1998; Stupp 2000) considered linear stage of the instability to specify the fastest growing wave-mode as a function of the plasma parameter

$$Y = \omega_{pe}/\omega_{Be}, \tag{1}$$

where ω_{pe} is the electron plasma frequency and ω_{Be} is the electron gyrofrequency. While the fundamental extraordinary mode (X1) was found to have the largest growth rate for $Y < 0.2 - 0.4$, other modes grow faster if $Y > 0.2 - 0.4$. Indeed, fundamental ordinary mode (O1) or second harmonics of either extraordinary (X2) or ordinary (O2) mode as well as one of unobservable plasma modes may display the largest growth rate value depending on the specific fast electron distribution. For example, if the angular gradient of the pitch-angle distribution peaks at small pitch-angles then O1 mode dominates at $Y < 1$, while if it peaks at large pitch-angles then X2 mode displays larger growth rates in this range (Winglee and Dulk 1986).

A particular attention has been paid to the role of gyroabsorption by the background coronal plasma in either emission source or along the ray path (in the harmonic gyrolayers) (Sharma et al. 1982; Sharma and Vlahos 1984). Anisotropic quasi-maxwellian distributions were found to be inefficient for ECM emission if the background plasma is hot enough, $T \gtrsim 10^7 K$ (Sharma and Vlahos 1984). The absorption in gyrolayers was found to represent a severe problem for the ECM emission to escape the corona (Sharma and Vlahos 1984), since the optical depth of the second gyrolayer calculated with the maxwellian background distribution is typically much larger than unity. However, estimates of nonlinear absorption (when the background distribution is modified by the incident powerful radiation) (Huang 1987) and particle-in-cell simulations (McKeen et al. 1990) show that even fundamental ECM emission has a chance to escape. Nevertheless, it remains unclear if the nonlinear absorption actually happens in solar conditions or not (and, accordingly, which harmonics can really escape the source to the observer).

Nonlinear stage of the ECM instability has also been studied both analytically and numerically. An elegant solution for (simplified) quasilinear equations was obtained for a quasi-maxwellian initial distribution (Wu et al. 1981) and it was later generalized (Pritchett 1986) to the case of DGH distribution (Dory et al. 1965). *One-dimensional* particle-in-cell simulations (Pritchett 1986) were found to agree well with the simplified analytical approach. The one-dimensional quasilinear saturation of the instability gives rise to a plateau formation in the distribution function of fast electrons over the transverse (to the magnetic field) velocity, providing, therefore, an absolute stabilization of the electron distribution. This means, that only the wave-mode with the largest growth rate can be amplified substantially, while weaker growing wave-modes remain practically unamplified.

The quasilinear relaxation is well known to occur rather differently for the *two-dimensional* case (Akhiezer et al. 1974) relevant to the ECM emission. Indeed, the relaxation due to the dominant mode affects the electron distribution in such a way that the new (modified) distribution is stable against this particular wave-mode. However, this new state is not necessarily stable against generation of other wave-modes, i.e., it is not absolutely stable distribution. Thus, other wave-modes can well continue to grow until they start to affect the electron distribution in their turn.

Two-dimensional fully relativistic numerical calculations of the ECM quasilinear relaxation (Aschwanden 1990) revealed many important properties of the relaxation process. However, only the fastest growing mode was included in the numerical code in that study. It is interesting, that even after 50 growth times this wave-mode is not completely saturated, while is still growing. The reason of this effect is not so trivial. Actually, the matter is that the initial distribution function selected for the calculations has artificially large angular gradient in the range of pitch-angles practically free from fast electrons (that is discussed in more detail in the next section). Respectively, the rate of the diffusion over the pitch-angles is rather low, while the growth rate of the amplified wave remains positive due to this artificial feature over a very long period of time.

Quasilinear relaxation was further studied numerically for a particular set of the involved parameters when the lower-hybrid wave-mode has the largest growth rate (Fleishman and Arzner 2000). The electron distribution is shown to remain clearly anisotropic after the relaxation against the lower-hybrid waves. The new anisotropic distribution is, however, stable against the lower-hybrid waves, although unstable against the electromagnetic wave-modes in agreement with the general results of the plasma physics (Akhiezer et al. 1974). In addition, the time profile of the generated wave energy density was found to resemble the observed spike time profiles (Güdel and Benz 1990). Nevertheless, the ECM saturation process has not been studied in detail yet, thus, additional studies of the quasilinear relaxation against electromagnetic wave-modes are necessary.

Although most of the studies were performed for a uniform plasma, the role of coronal inhomogeneities both in ECM source and at the ray path was analyzed. Effect of MHD-waves on the longitudinal transparency window (Robinson 1991a) and on the efficiency of the mode conversion (Robinson 1991b) was studied. Then, ECM line formation in either regularly or randomly inhomogeneous source was found to produce either spectral broadening or splitting of the initial peak depending on the strength of the inhomogeneity (Platonov and Fleishman 2001). Mutual action of regular coronal non-uniformity and random local inhomogeneities was considered for a beam-like electron distributions (Vlasov et al. 2002).

This paper studies the properties of the ECM growth rates produced by fast electrons with a power-law momentum distribution. While a few studies involving such distributions have already been done (Fleishman and Yastrebov 1994a; Fleishman and Yastrebov 1994c; Stupp 2000), the properties of the ECM instability from power-law distributions remain poorly established. Furthermore, a particular attention is paid to specify the pitch-angle distribution of the fast electrons consistently with the data obtained from other accompanying emissions, e.g., hard X-ray (HXR) and microwave continuum radiations, generated by the same or related populations of the fast electrons.

The paper is arranged as follows. Section 2 discusses the observational constraints available to restrict the shape of the involved distribution of the fast electrons over the momentum and pitch-angle. General formulation of the problem is given in section 3. Section 4 presents the results of the numerical calculations, and discussion is given in section 5.

2. Initial Electron Distribution

Let us discuss now the theoretical models used in the literature to describe the distribution function of fast electrons in the spike sources and observational data available to select the most realistic model for this distribution function. As a first approximation we consider a factorized distribution function

$$f(\mathbf{p}) = \frac{N_e}{2\pi} f_1(p) f_2(\mu). \tag{2}$$

The distribution function (2) is normalized by d^3p

$$\int f(\mathbf{p}) p^2 dp d\mu d\varphi = N_e, \tag{3}$$

where N_e is the number density of fast electrons, $\mu = cos\theta$, θ is the pitch-angle, φ is the azimuth angle, the specific distributions $f_1(p)$ and $f_2(p)$ are normalized as follows:

$$\int f_1(p) p^2 dp = 1, \qquad \int_{-1}^{1} f_2(\mu) d\mu = 1. \tag{4}$$

First of all, consider the correlations between spike bursts and HXR (Aschwanden and Güdel 1992). It is important that the solar radio spikes display a very high association rate with HXR flares, and many events reveal tight correlation between averaged spike radio flux and HXR flux. This correlation supports strongly a common source for the fast electrons producing HXR and radio spikes respectively.

The averaged spike flux is typically delayed by 2-5 s in respect to simultaneous HXR emission. Thus, the spikes are unlikely produced by beams of precipitating electrons or an up-reflected fraction of such beams (the typical time delay between type III bursts produced by beams and HXRs is less than 1 s). However, this time delay is easily interpreted if the radio spikes are generated by the fraction of fast electrons trapped in the magnetic loop (Fleishman and Melnikov 1998).

Then, the strongest correlation between spike flux and HXRs is observed when one considers the lowest energy HXR channel (Aschwanden and Güdel 1992). This means that relatively low-energy electrons ($E_{kin} < 100\ keV$ at least) are mainly responsible for the generation of the solar radio spikes. Therefore, any narrow distributions peaking at high energies ($E_{kin} > 100\ keV$) are irrelevant for radio spike production.

In addition, we should take into account that the spikes are only observed during the phase of a HXR burst with sufficiently hard spectrum ($\alpha_{HXR} < 6 - 7$) (Aschwanden and Güdel 1992). Obviously, this property should be reproduced within the appropriate spike emission model.

Further important information about the fast electron distribution can be obtained from the correlation between spike bursts and gyrosynchrotron microwave continuum (Fleishman et al. 2003).

The degree of polarization at the optically thin region of "spike-producing" microwave bursts was found to be systematically larger than for all other microwave continuum bursts (Fleishman et al. 2003). Obviously, this is an indication of rather non-symmetric magnetic structure at the source, as well as loss-cone-like angular distribution of the radiating electrons (Fleishman and Melnikov 2003).

The correlations between spike emission and microwave continuum are different depending on the viewing angle at which the microwave source is observed. For quasitransverse cases the averaged spike flux is the largest when the optically thin gyrosynchrotron emission has the hardest spectrum. For the quasitransverse case the hardest emission spectrum corresponds to the hardest spectrum of fast electrons accumulated at the loop (Fleishman and Melnikov 2003). Thus, the hard fast electron spectrum is favorable for the solar radio spike production – the same conclusion as from spike-HXR correlations.

However, for quasiparallel viewing angle of the gyrosynchrotron source the pitch-angle anisotropy (if present) can strongly affect the high-frequency spectral index of the microwave emission (specifically, the loss-cone anisotropy produce softer spectra than the isotropic distribution). Indeed, the high-frequency microwave emission of the spike-producing microwave bursts observed at a quasiparallel viewing angle is found to be much softer than for all other microwave bursts (and the spike-producing microwave bursts observed at a quasitransverse angle) (Fleishman et al. 2003).

The difference in the spectral indices for these two classes of spike-producing microwave bursts is as high as 3-4. It is remarkable that for the quasiparallel case the softest gyrosynchrotron spectra (read the most anisotropic distribution of fast electrons) are favorable for spike generation.

We, thus, can conclude that the observations are strongly in favour of loss-cone distributions of fast electrons at the spike sources (rather than beam-like distributions) and summarize the requirements for the "test" pitch-angle distribution of fast electrons (the distribution over momentum is evidently a kind of power-law).

Indeed, the distribution must be able to provide the observed difference of 3-4 between the optically thin gyrosynchrotron spectra produced at quasitransverse and quasiparallel angles respectively. Then, the distribution should be able to provide the instability through the entire range of the spectral indices of the fast electron distribution over momentum occurred when the solar radio spikes are generated. And, finally, the efficiency of the instability (the typical values of the growth rate) should clearly decrease with the increase of the fast electron spectral index value as follows from spike-to-HXR (Aschwanden and Güdel 1992) and spike-to-microwave (Fleishman et al. 2003) correlations.

These requirements suggested by observations really allow to restrict the type of pitch-angle distribution of fast electrons producing the spike emission via ECM mechanism. Fig. 1 presents four different models for the angular distribution: gaussian (used in (Fleishman and Yastrebov 1994a; Fleishman and Yastrebov 1994c))

$$f_2(\mu) \propto exp(-\mu^2/\mu_0^2), \tag{5}$$

loss-cone with sinN function (used, e.g., in (Aschwanden 1990))

$$f_2(\mu) \propto \begin{cases} \sin^N\left(\frac{\pi}{2}\frac{\theta}{\theta_c}\right), & 0 < \theta < \theta_c, \\ 1, & \theta_c < \theta < \pi - \theta_c, \\ \sin^N\left(\frac{\pi(\theta-\pi)}{2\theta_c}\right), & \pi - \theta_c < \theta < \pi, \end{cases} \tag{6}$$

exponential loss-cone (used in (Fleishman 2003))

$$f_2(\mu) \propto \begin{cases} \exp\left(-\frac{\mu-\cos\theta_c}{\Delta\mu}\right), & \mu > \cos\theta_c, \\ 1, & -\cos\theta_c < \mu < \cos\theta_c \\ \exp\left(\frac{\mu+\cos\theta_c}{\Delta\mu}\right), & \mu < -\cos\theta_c, \end{cases} \tag{7}$$

and gaussian loss-cone

$$f_2(\mu) \propto \begin{cases} \exp\left(-\left(\frac{\mu-\cos\theta_c}{\Delta\mu}\right)^2\right), & \mu > \cos\theta_c, \\ 1, & -\cos\theta_c < \mu < \cos\theta_c \\ \exp\left(-\left(\frac{\mu+\cos\theta_c}{\Delta\mu}\right)^2\right), & \mu < -\cos\theta_c. \end{cases} \tag{8}$$

The function described the idealized loss-cone (used in (Stupp 2000))

$$f_2(\mu) \propto \left\{ \begin{array}{cc} 1, & \mu < cos\theta_c, \\ \frac{cos(\theta_c-\Delta\theta_c)-\mu}{cos(\theta_c-\Delta\theta_c)-cos\theta_c}, & cos\theta_c < \mu < cos(\theta_c-\Delta\theta_c), \\ 0, & \mu > cos(\theta_c-\Delta\theta_c) \end{array} \right. \tag{9}$$

is not shown in the figure because of its extremely simple shape.

Let us consider these angular distributions in more detail. The gaussian angular distribution (5) can provide the observed difference in spectral indices of optically thin gyrosynchrotron emission at quasiparallel and quasitransverse directions (Fleishman and Melnikov 2003) and the decrease of ECM efficiency for softer electron spectra (Fleishman and Yastrebov 1994a; Fleishman and Yastrebov 1994c). However, the instability disappears already for moderate values of spectral indices in the electron distribution over momentum, $\gamma \gtrsim 8$ and/or for extended power-law spectra with $p/mc > 1$
(Fleishman and Yastrebov 1994a; Fleishman and Yastrebov 1994c), which does not agree with observations.

This happens because the instability related to the gaussian angular distribution is rather weak being only slightly above the threshold. The efficiency of the instability is defined by relative importance of negative derivative of the distribution function over the momentum modulus and positive contribution related to angular gradient, which can be quantitatively described by the ratio of the angular gradient of the pitch-angle distribution to the angular distribution function itself. Although the angular derivative is not small, Fig. 1b, the peak value occurs at those angles where the angular distribution function is large, the ratio of these values is, therefore, small everywhere, Fig. 1c.

SinN angular distribution (6) has very different properties. While this function looks rather smoothed (it is continuous function together with its first derivative) and, thus, attractive for the use in theoretical calculations, it cannot be considered as a good approximation for the angular distribution of spike-producing fast electrons. First of all, the difference in spectral indices of optically thin gyrosynchrotron emission at quasiparallel and quasitransverse directions is typically less than unity for this distribution (Fleishman and Melnikov 2003) that is not sufficient to explain the observed difference of 3-4.

Moreover, this function has a very deep intrinsic problem. Indeed, if we compare the behavior of the function and its first derivative, Fig. 1a-b, we discover that the derivative decreases (with the decrease of the pitch-angle) much more slowly than the function itself. Particularly, the arrows in Fig. 1 indicate the region where the derivative is of order of unity, while the function is much less than unity. Note, that the ratio (Fig. 1c) diverges as the pitch-angle decreases. Thus, sinN function describes the case of the instability operating significantly above the respective threshold for any parameters of the function (6). As a result, the instability exists for any shape of the momentum distribution of fast electrons, and its efficiency has extremely weak dependence on the electron spectral index.

This artificial property has already produced a few unexpected and poorly understood results. In particular, the detailed numerical calculations of the ECM quasilinear saturation (Aschwanden 1990) did not ensure the entire maser saturation even after 50 growth times: the peak value of the growth rate was reduced by less than one order of magnitude for this time. The reason for this surprising behavior is rather slow angular diffusion in the range of small pitch-angles, where the distribution function is small but the angular gradient is sufficiently large to provide the instability and then support it for quite a long time. The quasilinear relaxation occurs differently if the instability operates closer to its threshold (Fleishman and Arzner 2000). The idealized loss-cone (9) has a similar problem.

Exponential loss-cone function (7) is free from such kind of problem. From the theoretical point of view it has the only disadvantage that is discontinuity of its first derivative at $\theta = \theta_c$. ECM produced by this function is studied in a companion paper (Fleishman 2003). This distribution ensures easily the instability through the entire range of required spectral indices and correct dependence of the ECM efficiency on the spectral index. However, the exponential decrease of the number of electrons in the loss-cone turns to be too slow to provide the observed difference of 3-4 in spectral indices of optically thin gyrosynchrotron emission at quasiparallel and quasitransverse directions. The gyrosynchrotron emission calculated for this distribution is shown in Fig.2, right column. One can see easily that the variation of the optically thin spectral index related to the pitch-angle anisotropy is less than 1.5 for this case.

Alternatively, a similar loss-cone distribution but with faster, gaussian, decrease of the number of electrons in the loss-cone (8) can evidently provide the required difference in the optically thin spectral indices, Fig. 2, left column. One can also note, that the gaussian loss-cone distribution provides stronger degree of polarization in the optically thin range than the exponential loss-cone distribution. It is worth emphasizing that in both cases the electron distribution used to calculate the gyrosynchrotron emission is not far from the corresponding marginal stability state.

The gaussian loss-cone function is attractive from the theoretical point of view, since it is a function continuous together with its first derivative. Our study proves that this function fits any other requirements suggested by spike observations.

Then, the distribution over the momentum was taken in the form:

$$f_1(p) \propto \begin{cases} \frac{(\gamma-3)p_0^{\gamma-3}}{p^\gamma}, & p_0 < p < p_{br}, \\ \frac{(\gamma-3)p_0^{\gamma-3}}{p_{br}^\gamma} \exp\left(-\gamma \frac{p-p_{br}}{p_{br}}\right), & p > p_{br}. \end{cases} \quad (10)$$

The normalization coefficient is approximately calculated under the assumption of broad ($p_0 << p_{br}$) spectrum with $\gamma > 3$. The shape of the exponential cut-off is selected in such a way that provides continuity of the distribution function and its first derivative at the break point p_{br}.

3. General formulation

This paper calculates growth rates of ordinary and extraordinary wave-modes close to a few lowest harmonics of the gyrofrequency. The spatial growth rates are defined as gyrosynchrotron absorption coefficients $\varkappa$ (the expression for $\varkappa$ and other relevant definitions are given in the Appendix) taken with the minus sign.

We calculate only the contribution provided by energetic electrons and neglect the background plasma contribution to the growth rates (although the wave dispersion is entirely controlled by the background plasma). The role of the thermal plasma is well studied in the literature. First of all, it provides gyroabsorption at a closed vicinity of the gyrofrequency and a few its first integer multiples. This thermal gyroabsorption may entirely suppress the ECM instability in narrow frequency ranges around the harmonics (Sharma and Vlahos 1984; Stupp 2000). The width of the absorption bands increases as the plasma electron temperature increases.

The effect of gyroabsorption at the source was found to be important if the energetic electrons have a maxwellian distribution. However, for the power-law distribution adopted for the current calculations the frequency range occupied by ECM instability is remarkably wide, Fig. 3, thus, the gyroabsorption is not very important, since it suppress the instability at quite a small part (at best) of the entire instability region. Therefore, the results obtained below should not change noticeably if one takes into account the gyroabsorption at the source.

The second important issue is the applicability of the cold plasma approximation (magneto-ionic theory) to describe the wave dispersion. The topic was discussed in detail in (Stupp 2000) for the ECM problem. This approximation may be incorrect in a narrow vicinity of the gyroharmonics. Thus, we can neglect any thermal corrections to the wave dispersion, since we have already discarded the gyroabsorption at the source that is effective in the very same frequency band. Therefore, our treatment is correct everywhere except a few narrow bands around the lowest gyroharmonics, whose bandwidth increases as the temperature grows.

Then, the gyroabsorption at the harmonic layers (Sharma et al. 1982) can prevent the amplified radiation to escape the source to the observer. Although the problem has not been firmly solved yet in the literature, there are commonly accepted agreement that the second (and higher) harmonic radiation have a good chance to escape the third (and higher) gyrolayers (Sharma et al. 1982). Moreover, nonlinear absorption may reduce significantly the optical depth of the second gyrolayer and make it more transparent for the fundamental emission (McKeen et al. 1990). We rely on the cited papers and do not pay much further attention to this problem.

Since we consider quite a broad energy spectrum, we use the fully relativistic equations for the spatial growth rates and related quantities; below we study the dependence of the growth rates on the plasma density and parameters of the test electron distribution function.

4. Numerical results

The basic calculations of the value of the growth rate for a fixed direction at a given frequency were organized in a straightforward way: numerical integration with the gaussian routine followed by summation of the series over n. Exact expressions for the Bessel functions and recurrent expressions for their derivatives were used. The numerical accuracy was typically 1%.

The growth rates were calculated on the greed with the angular spacing of about 1^o and the step in frequency $\Delta\omega = 10^{-3}\omega$. Then, the absolute maximum of the growth rate for each wave-mode at the ranges of fundamental, second and third harmonics was found. This maximum was considered as the peak value for a selected set of incoming parameters.

4.1. Basic parameters.

The growth rate value depends on many parameters, therefore, we first selected a set of basic parameters and then varied each of them successively. This approach allows to discuss properly what effect is produced by each particular parameter.

For our calculations we selected two basic values of the plasma frequency to gyrofrequency ratio, $Y = \omega_{pe}/\omega_{Be} = 1,\ 1.3$. When $Y = 1$, the most rapid growth of the extraordinary waves occurs at the second harmonics, $s = \omega/\omega_{Be} \approx 2$, while of the ordinary waves at the fundamental, $s \approx 1$. Thus, we can compare the properties of X2 and O1 growth rates respectively. For $Y = 1.3$ the growth of O1 waves becomes ineffective, so we deal with X2 and O2 waves. We do not consider extremely small Y values when X1 waves can grow effectively because it is doubtful that such low values can actually exist in solar flares.

The angular distribution of fast electrons depends on two parameters in case of model function (8): loss-cone angle θ_c and the width of the distribution $\Delta\mu$. We selected $\theta_c = 60^o$ and $\Delta\mu = 0.15$. The later value allows the instability to operate in the moderately-above-threshold regime.

For the basic distribution of fast electrons over momentum we selected the following parameters typical for flares: $p_0/mc = 0.2$ ($E_{kin} \approx 10\ keV$), $p_{br}/mc = 3$ ($E_{kin} \approx 1.1\ MeV$) and $\gamma = 6$.

4.2. Effect of plasma density.

The effect of plasma density on the growth rates of the lowest harmonics of the gyrofrequency was repeatedly studied for various electron distributions (Sharma et al. 1982; Sharma and Vlahos 1984; Li 1986; Winglee and Dulk 1986; Aschwanden 1990) (Fleishman and Yastrebov 1994a; Fleishman and Yastrebov 1994c; Ledenev 1998; Stupp 2000). It is well-known that for small $Y < 0.2-0.4$ the fundamental extraordinary waves (X1) have the largest growth rates. Then, for larger Y, the amplification of X1 waves becomes inefficient and other waves become dominant (O1, X2, ...). Our calculations agree well with this standard picture (since it is largely related to kinematic restrictions).

The dependence of the growth rates on Y (for the adopted power-law momentum distribution and gaussian loss-cone angular distribution) in the limits $0.1 < Y < 2.5$ is given by Fig.4: the left column corresponds to $\gamma = 6$ and the right column corresponds to $\gamma = 8$, three loss-cone angle values were used: $\theta_c = 45^o,\ 60^o,\ 75^o$ for the top, middle and bottom panels respectively.

The growth rate of each harmonics decreases rapidly when the cut-off frequency of corresponding wave-mode exceeds the respective multiple of gyrofrequency (i.e., when $Y > 1$ for O1 waves, $Y > \sqrt{2}$ for X2 waves, $Y > 2$ for O2 waves etc). The absolute peak of the growth rate at a particular harmonics of the extraordinary waves is noticeably larger than of ordinary waves at the same harmonics. The absolute peak value decreases as the harmonic number increases.

The range of Y variation where a wave-mode is the fastest growing mode depends on parameters of the fast electron distribution. In particular, for small loss-cone angle value (top), the growth rates of O1 waves are larger than of X2 waves for $Y < 1$. However, the difference between them decreases as θ_c increases (middle) and X2 waves grow faster than O1 waves for large θ_c (bottom) in agreement with the finding of (Winglee and Dulk 1986). Respectively, O1 mode grows faster than X2 mode if $Y < 1$ for $\theta_c = 45^o$, if $Y < 0.85$ for $\theta_c = 60^o$, and never for $\theta_c = 75^o$. Then, for $Y > \sqrt{2}$ the O2 mode is the dominant, and for $Y > 1.8$ the X3 mode may dominate (if it is unstable for a particular set of parameters).

We note an interesting feature specific for our electron distribution: the amplification of the third harmonics of both extraordinary and ordinary waves is ineffective for hard electron spectra (e.g., $\gamma = 6$, left column) for most of the Y range, while it is effective for softer spectra (e.g., $\gamma = 8$, right column). The reason for the instability suppression for the hard spectrum is the destructive contribution of (true absorption by) high-energy electrons. For softer electron distributions the role of high-energy electrons is less important allowing the instability at the third harmonics. Note that for the gaussian angular distribution (5) used in (Fleishman and Yastrebov 1994a; Fleishman and Yastrebov 1994c), the instability suppression by high-energy tail of power-law distribution is important even at the fundamental and second harmonics, since the gaussian distribution provides weaker angular gradients than considered here gaussian loss-cone distribution (8).

4.3. Effect of angular distribution.

The adopted pitch-angle distribution (8) depends on two parameters: loss-cone angle θ_c and width of the distribution $\Delta\mu$.

The dependences of the maximized (over the emission frequency and angle) spatial growth rates for X2, O1 and O2 waves are shown in Fig. 5. All the curves are bell-shaped. The most effective amplification of O1 waves occurs around $\theta_c \approx 45^o$, while around $\theta_c \approx 60^o$ for O2 waves and even higher values for X2 waves. No qualitative difference is seen for various electron spectral indices γ.

Let us discuss in more detail the dependences on the width of the distribution $\Delta\mu$, Fig. 6. Evidently, all the growth rates increase as $\Delta\mu$ decreases because this corresponds to stronger angular gradients, and, thus, to stronger instability. However, the growth rates decrease as $\Delta\mu$ increases first gradually and then rapidly. This rapid decrease occurs when the instability approaches its threshold provided by negative contribution of the momentum term ($\partial f/\partial p = -\gamma f$). When $\Delta\mu$ exceeds $0.1 - 0.3$ (depending on other parameters) the instability disappears. We emphasize that this happens when the pitch-angle distribution of fast electrons remains clearly anisotropic. Thus, such anisotropic distributions can generate standard gyrosynchrotron emission without coherent ECM emission.

The detailed shape of the curves depends on other parameters, like Y and θ_c. For X2 and O2 waves, large θ_c values are preferable, while for O1 waves - lower θ_c values. However, for all considered cases, $\theta_c = 60^o$ has the largest threshold $\Delta\mu$ value.

4.4. Effect of distribution over momentum.

The adopted distribution over modulus of momentum depends on three parameters: the minimal momentum p_0, the break-point p_{br} where the power-law is giving way to the exponential cut-off, and the electron spectral index γ.

The growth rates of all considered wave-modes display rather weak dependence on p_{br} for the selected set of basic parameters, so we do not present the corresponding plots. We should note, however, that this property of the ECM emission is model-dependent and valid if the instability operates noticeably above the threshold. If the instability is very close to its threshold, the behavior of the momentum distribution in the high-energy range may be important. In particular, this is the case of gaussian pitch-angle distribution (Fleishman and Yastrebov 1994a; Fleishman and Yastrebov 1994c).

The dependence of the growth rates on the minimal momentum p_0 is shown in Fig. 7. Shape of the curves is clearly different for various harmonics and wave-modes. X2 waves display decreasing curves with increasing p_0, thus, low-energy electrons are preferable to produce these waves. Wide loss-cones ($\theta_c = 60^o$, 75^o) provide larger growth rates than narrower loss-cone ($\theta_c = 45^o$).

Ordinary waves are generated most effectively if the low-energy cut-off is about 20 keV for O2-mode and about 10 keV for O2 mode. Narrow loss-cone ($\theta_c = 45^o$) is the most efficient to produce O1 waves and wider one ($\theta_c = 60^o$) is preferable to produce O2 waves. The wide loss-cone of $\theta_c = 75^o$ is less effective for the both first harmonics of the ordinary waves.

Considering together the plots in Fig.7, one can conclude that different fractions of fast electrons are responsible for generation of these different wave-modes. Thus, quasilinear relaxation against one (the dominant) mode should not necessarily provide saturation of all other wave-modes in agreement with numerical quasilinear simulations (Fleishman and Arzner 2000).

Of particular importance are the dependences of the growth rates on the electron spectral index γ, since they can be compared with the observational data obtained from the analysis of correlations between spike bursts and continuum (microwave and HXR) emissions.

All the curves shown in Fig.8 are bell-shaped; peak of each curve corresponds to a favourable γ value specific for each wave-mode. The decrease of the growth rates for harder spectra (smaller γ) is provided by negative contribution of high-energy electrons at large harmonics. The decrease for softer spectra (larger γ) is related to the increase of the instability threshold that is proportional to γ for the power-law momentum distribution of the electrons.

The favourable γ value depends on the harmonic number and type of the wave. X2 waves display the dependences with the peak around $\gamma = 6$ (which corresponds to the synchrotron spectrum with the index 1.5) for a broad range of the involved parameters. A bit lower values are favourable for O2 waves. However, O1 waves display the peak at rather small values $\gamma = 4 - 5$.

It is remarkable that the favourable γ values for the third harmonics are significantly larger than for the fundamental and second harmonics: it is about 8 (synchrotron spectral index 2.5) for O3 waves and even larger for X3 waves. Such a different behavior of the curves for the different waves can in principle be used to specify the contribution of various harmonics to the spike radiation. However, this tasks requires the data with exceptional quality that is not available currently. So far, it is found that hard electron spectra are favourable for spike generation (Aschwanden and Güdel 1992; Fleishman et al. 2003), the range of the electron spectral indices is typically restricted by the values $\gamma > 6$.

5. Discussion

The paper discusses in some detail the properties of the ECM instability provided by fast electrons with distribution function specified with the use of available observational data: the power-law distribution over momentum is consistent with spectral properties of microwave and HXR emission accompanying the spike bursts, while the pitch-angle distribution is taken in a form consistent with the difference of gyrosynchrotron spectral indices of the microwave sources (accompanying the spike bursts) observed at a quasitransverse and quasiparallel to the magnetic field directions respectively.

We emphasize that the properties of ECM growth rates agree well with many observed properties of solar millisecond radio spikes. First of all, the decrease of the growth rates with the γ increase corresponds to smaller efficiency of the ECM emission for softer spectra of fast electrons. The correlation of this type is actually observed when spectra of microwave or HXR emission simultaneous to spike bursts are analyzed: the harder the fast electron spectrum the stronger the averaged spike flux. The range of microwave spectral indices is $\alpha = 1 - 4$ typically. Thus, we can conclude that most of the spikes are generated at a harmonics not larger than second. Indeed (see Fig. 8), ECM emission at the third harmonics is the most efficient if $\gamma \approx 8$ ($\alpha \approx 2.5$), therefore, the softer microwave spectra should be preferable for spike generation in the range $\alpha < 2.5$, which is not observed.

However, the observational data about spike-to-microwave continuum correlations is not very numerous and precise yet, so we cannot entirely exclude a contribution from the third ECM harmonics. Potentially, the study of spike-to-microwave continuum correlations may put important constraints on the harmonics operating at the spike bursts.

Secondly, the dependences of the growth rates on the low-energy cut-off value (p_0) agrees well with the discovered type of correlation between HXRs and spike bursts: the lowest energy HXR channel displays the best correlation with the averaged spike flux.

Thirdly, the dependences on the angular gradient value ($\Delta\mu$) display clearly that (as $\Delta\mu$ increases) the instability disappears when the pitch-angle distribution remains still evidently anisotropic ($\Delta\mu = 0.2 - 0.3$). Accordingly, the overall distribution of fast electrons accumulated at the loop may be rather anisotropic for a long time providing noticeably softer gyrosynchrotron spectra (for a quasiparallel viewing angle) than the isotropic distribution, which is observed indeed (Fleishman et al. 2003).

Let us further discuss what conclusions can be made about the harmonics and wave-mode giving the main contribution to the solar radio spike emission. The polarization data is important evidently for this purpose. While there is important evidence in favour of preferable X-mode spike polarization (Güdel and Zlobec 1991; Fleishman et al. 2003), the problem has not been finally solved yet. Thus, O-mode contribution cannot be currently excluded by observations.

An important parameter to evaluate the ECM efficiency is the amplification (e-folding) length. The scale of a single spike source is estimated (indirectly) as $\sim 200\ km$ (Benz 1985); a wave should experience many e-folding amplifications over this length to produce observable spike with large brightness temperature, so this requirement reads $\varkappa \gg 5 \cdot 10^{-8} cm^{-1}$. The amplification coefficient (spatial growth rate) in the dimension form is

$$\varkappa_\sigma(\omega, \vartheta) = \frac{\pi\omega_{Be}}{2c}\frac{N_e}{N}\varkappa_\sigma^{num}(\omega, \vartheta), \tag{11}$$

where $\varkappa_\sigma^{num}$ is presented in the plots. For the gyrofrequency $\omega_{Be} = 2\pi \times 1\ GHz$ we have

$$\varkappa_\sigma = 0.33\frac{N_e}{N}\varkappa_\sigma^{num}. \tag{12}$$

We conclude that the required amplification can easily by provided for the fundamental and second harmonics of both X- and O- modes. Moreover, the amplification of X3 mode is also possible if fast particles are numerous enough, $N_e/N \gtrsim 10^{-2}$, while the amplification of O3 mode is less probable.

Additional constraints to the particular wave-mode mainly contributing to the spike emission can be obtained from temporal properties of millisecond spikes. Indeed, the spike duration is largely function of emission frequency with rather weak scatter around the regression curve (Güdel and Benz 1990; Meszarosova et al. 2002), see also Fig. 9 gathering all currently available measurements of spike duration. The regression low found from this figure for the entire available spectral range, 237-2695 MHz,

$$\tau \propto f^{-1.29\pm0.08}, \tag{13}$$

is compatible with that established by (Güdel and Benz 1990) for a restricted spectral range.

Since we can expect the Y value to have a rather broad distribution in the solar corona, then only those harmonics that display rather gradual dependence of the growth rate on Y are the candidates to spike-producing wave-mode. This clearly excludes the X1 mode from the list because it has very strong dependence on Y (Fig. 4). The minor role of X1 waves in spike generation may be related to either seldom small Y (< 0.3) values in the corona or gyroabsorption of X1 waves at the second gyrolayer.

To proceed further we need to discuss the dependence of temporal (rather than spatial) growth rates on Y. Indeed, within the quasilinear approach, the ECM pulse duration is inversely proportional to the characteristic growth rate value Γ:

$$\tau \propto \Gamma^{-1}. \tag{14}$$

The growth rate

$$\Gamma_\sigma = v_\sigma \varkappa_\sigma = \omega_{Be} \frac{\pi N_e}{2N} \Gamma_\sigma^{num}, \tag{15}$$

where v_σ is the group velocity of the σ waves (evidently, $\Gamma_\sigma^{num} = v_\sigma \varkappa_\sigma / c$), depends on Y for each particular wave-mode . Since the ECM emission frequency is proportional to gyrofrequency at the source, $\omega = s\omega_{Be}$, it is reasonable to expect that $Y = \omega_{pe}/\omega_{Be}$ decreases (on average) as the frequency (and gyrofrequency) increases. If the dimensionless growth rate Γ^{num} for a particular harmonics does not depend on Y (in some limited range), the ECM pulse duration is proportional to f^{-1} ($f = \omega/2\pi$) flatter than the observed law (13). The observed law can only be obtained if solar radio spikes are produced preferably at the range of parameters providing slow decrease of the growth rate Γ^{num} with Y increase.

Fig. 10 displays the dependences of the temporal growth rates Γ^{num} for the first three harmonics on Y. If we take into account only those ranges of Y variation where a given wave-mode has the largest growth rate, we find that O1 mode displays mainly growing with

Y curves, which is incompatible with the observed law (13), while X2, O2, and X3 modes contain falling parts, which might be consistent with the observed law (13).

As an example, consider a part of the curve for X2 mode where this mode has the largest growth rate. Fig. 11 displays an enlarged part of the curve. The best fit by the linear function (in the logarithmic scale) gives the approximation $\Gamma^{num} \propto Y^{-0.28}$ with deviations from this law of about $20-30\%$. For dimension values we, therefore, have $\Gamma \propto \omega_{Be}^{1.28}$, and finally for the duration we find $\tau \propto f^{-1.28}$ with $20-30\%$ scatter in agreement with observations.

The same analysis of O2 mode gives steeper law than observed for spikes. Thus, we conclude that X2 mode is the best candidate to produce the majority of millisecond spikes. However, this does not mean that radiation of other harmonics of extraordinary and ordinary mode is entirely unimportant: we emphasize the importance of further analysis of observations, which might provide us with more detailed new information about actual contribution of different harmonics to the observed radio emission.

We conclude that the ECM instability produced by fast electrons with realistic (determined from observations) distributions over momentum and pitch-angle is naturally able to generate radio emission with the properties typical for millisecond solar radio spikes. Moreover, the analysis shows that most of the spikes are produced most probably as X2 waves.

I am strongly grateful to Paolo Zlobec for exceedingly helpful discussions about many spike properties and for his valuable comments about spike duration. The work was supported by the Russian Foundation for Basic Research, grants No.02-02-39005, 03-02-17218, and Chinese NFS projects No.10273025, "973" program with No.G2000078403.

Appendix

The spatial growth rate (self-absorption coefficient taken with the minus sign) have the form (Eidman 1958; Eidman 1959; Ramaty 1969):

$$\begin{gathered}
\varkappa_\sigma(\omega,\vartheta) = \frac{\pi\omega_{pe}^2}{(1+K_\sigma^2+\Gamma_\sigma^2)\left(2n_\sigma\frac{\partial(\omega n_\sigma)}{\partial\omega}\right)v_\sigma N} \\
\sum_{n=1}^{\infty}\int d^3p(1-\mu^2) \\
\left[\frac{-\Gamma_\sigma\sqrt{1-\eta^2}+K_\sigma(\eta-\beta\mu n_\sigma)}{n_\sigma\beta\sqrt{(1-\mu^2)(1-\eta^2)}}J_n(z)+J_n'(z)\right]^2 \\
\left[p\frac{\partial}{\partial p}-(\mu-n_\sigma\beta\eta)\frac{\partial}{\partial\mu}\right]f(\mathbf{p}) \\
\delta(\gamma_e\omega-n\omega_{Be}-\gamma_e\beta n_\sigma\eta\mu\omega)
\end{gathered} \tag{1}$$

where $f(\mathbf{p})$ is the distribution function (2) of fast electrons, ω_{pe} and ω_{Be} are the electron plasma- and gyrofrequencies, N is the number density of the background plasma, $\eta = cos\vartheta$, ϑ is the view angle, $J_n(z)$ and $J_n'(z)$ are the Bessel function and its derivative over argument z, $z = (\omega/\omega_{Be})\gamma_e n_\sigma \beta\sqrt{(1-\mu^2)(1-\eta^2)}$, $\beta = v/c$ is the dimensionless particle velocity, v_σ is the group velocity of the σ-mode wave.

The polarization vector $\mathbf{e}_{\sigma,\mathbf{k}}$ of σ-mode wave ($\sigma = 1$ for O-mode and $\sigma = -1$ for X-mode) in the reference frame with z-axes along the magnetic field $\mathbf{B}$ and $\mathbf{k}$-vector in the $(y,\ z)$ plane is

$$\mathbf{e}_{\sigma,\mathbf{k}} = \frac{(1,\ i\alpha_\sigma,\ i\beta_\sigma)}{(1+\alpha_\sigma^2+\beta_\sigma^2)^{1/2}} \tag{2}$$

where

$$\alpha_\sigma = K_\sigma cos\vartheta - \Gamma_\sigma sin\vartheta, \quad \beta_\sigma = K_\sigma sin\vartheta + \Gamma_\sigma cos\vartheta \tag{3}$$

$$K_\sigma = \frac{2\sqrt{u}(1-v)cos\vartheta}{usin^2\vartheta - \sigma(u^2 sin^4\vartheta + 4u(1-v)^2 cos^2\vartheta)^{1/2}}, \quad K_X K_O = -1 \tag{4}$$

$$\Gamma_\sigma = -\frac{v\sqrt{u}sin\vartheta + uvK_\sigma cos\vartheta sin\vartheta}{1-u-v(1-ucos^2\vartheta)} \tag{5}$$

$$v = \omega_{pe}^2/\omega^2, \qquad u = \omega_{Be}^2/\omega^2. \tag{6}$$

The refractive indices have the form:

$$n_\sigma^2 = 1 - \frac{2v(1-v)}{2(1-v) - u\sin^2\vartheta + \sigma(u^2\sin^4\vartheta + 4u(1-v)^2\cos^2\vartheta)^{1/2}} \tag{7}$$

Before doing the numerical calculations the integrals over the azimuth angle ϕ and over μ in (1) were taken analytically (with the use of δ-function). After the integration we have:

$$\varkappa_\sigma(\omega,\vartheta) = -\frac{\pi^2\omega_{pe}^2}{\omega|\eta|v_\sigma N(1+K_\sigma^2+\Gamma_\sigma^2)\left(n_\sigma^2\frac{\partial(\omega n_\sigma)}{\partial\omega}\right)} \sum_{n=1}^{\infty}\int\frac{p^2}{\gamma_e\beta}dp(1-\mu^2) \left[\frac{-\Gamma_\sigma\sqrt{1-\eta^2}+K_\sigma(\eta-\beta\mu n_\sigma)}{n_\sigma\beta\sqrt{(1-\mu^2)(1-\eta^2)}}J_n(z)+J_n'(z)\right]^2 \left[p\frac{\partial}{\partial p}-(\mu-n_\sigma\beta\eta)\frac{\partial}{\partial\mu}\right]f(\mathbf{p})|_{\mu=\mu_*}, \tag{8}$$

where

$$\mu_* = \frac{\gamma_e\omega - n\omega_{Be}}{\gamma_e\beta n_\sigma\eta\omega}, \qquad |\mu_*| \le 1. \tag{9}$$

The respective dimensionless value $\varkappa_\sigma^{num}(\omega,\vartheta)$ (the normalization is described in the main text, Eq. (11)) were calculated numerically after substituting the distribution function (2) of fast electrons.

REFERENCES

Akhiezer, A.I., Akhiezer, I.A., Polovin, R.V., Sitenko, A.G., and Stepanov, K.N. Plasma Electrodynamics, (Ed. -A.I.Akhiezer), Moscow, Nauka 1974 (Pergamon, Oxford, 1975)

Aschwanden, M.J. 1990, A&AS, 85, 1141

Aschwanden, M.J. and Benz, A.O. 1988, ApJ, 332, 447

Aschwanden, M.J., and Güdel, M. 1992 ApJ, 401, 736

Barrow, C.H., Zarka, P., and Aubier, M.G., 1994 A&A, 286, 597

Benz, A.O. 1985, Sol. Phys., 96, 357

Dory, R.A., Guest, G.E., and Harris, E.G. 1965, Phys. Rev. Lett., 14, 131

Eidman, V.Ya. 1958, Sov. Phys. JETP, 7, 91

Eidman, V.Ya. 1959, Sov. Phys. JETP, 9, 947

Fleishman, G.D. 1994, Sol. Phys., 153, 367

Fleishman, G.D. 2003, Astron Repts. (submitted)

Fleishman, G.D., and Arzner, K. 2000, A&A, 358, 776

Fleishman, G.D., Gary, D.E., and Nita, G.M. 2003, ApJ, 593,

Fleishman, G.D., and Melnikov, V.F. 1998, Physics - Uspekhi, 41, 1157

Fleishman, G.D., and Melnikov, V.F. 2003, ApJ, 587, 823

Fleishman, G.D., and Yastrebov, S.G. 1994a, Sol. Phys., 153, 389

Fleishman, G.D., and Yastrebov, S.G. 1994b, Sol. Phys., 154, 361

Fleishman, G.D., and Yastrebov, S.G. 1994c, Astron. Zhurn., 71, 531

Güdel, M., and Benz, A.O. 1990, A&A, 231, 202

Güdel, M., and Zlobec, P. 1991, A&A, 245, 299

Harris, E.G. 1959, Phys. Rev. Lett., 2, 34

Holman, G.D., Eichler, D., and Kundu, M.R. 1980, in Radiophysics of the Sun (Eds M.R.Kundu, T.E.Gergely)(Dordrecht: Reidel, 1980) p.457.

Huang, G.-L. 1987, Sol. Phys., 114, 363

Ledenev, V.G. 1998, Sol. Phys., 179, 405

Li, H.W. 1986, Sol. Phys., 104, 131

Lipatov, B.N., Melnikov, V.F., Podstrigach, T.S., Snegirev, S.D., Tikhomirov, Yu.V., Fridman, V.M., and Sheiner, O.A. 2002, Radiophys. and Quantum Electr., 45, 75

McKeen, M.E., Winglee, R.R., and Dulk, G.A. 1990 in Proc. of 3th Workshop Max'91 Solar Flares (Eds. R.R.Winglee and A.L.Kiplinger), Colorado, Boulder, p.29

Melrose, D.B., and Dulk, G.A. 1982, ApJ, 259, 844

Meszarosova, H., Veronig, A., Zlobec, P., and Karlicky, M. 2002 Proc. 10^{th} European Solar Physics Meeting, 'Solar Variability: From Core to Outer Frontiers', Prague, Czech Republic, 9-14 September 2002 (ESA SP-506, December 2002), 1, 347.

Platonov, K.Yu., and Fleishman, G.D. 2001, Astron. Repts., 45, 203

Pritchett, P.L. 1986, Phys. Fluids, 29, 2919

Ramaty, R. 1969, ApJ, 158, 753

Robinson, P.A. 1991a, Sol. Phys., 134, 299

Robinson, P.A. 1991b, Sol. Phys., 136, 343

Sagdeev, R.Z., and Shafranov, V.Ts. 1960, ZhETF, 39, 181 (transl.: 1961, Sov. Phys. - JETP, 12, 130)

Schneider, J. 1959, Phys. Rev. Lett., 2, 504

Sharma, R.R., and Vlahos, L. 1984, ApJ, 280, 405

Sharma, R.R., Vlahos, L., and Papadopoulos, K. 1982, A&A, 112, 377

Stepanov, A.V. 1978, Pis'ma v Astron. Zh., 4, 193

Stupp, A. 2000, MNRAS, 311, 251

Twiss, R.Q. 1958, Austral. J. Phys., 11, 564

Vlasov, V.G., Kuznetsov, A.A., and Altyntsev, A.T. 2002, A&A, 382, 361

Winglee, R.R., and Dulk, G.A. 1986, Sol. Phys., 104, 93

Winglee, R.R., Dulk, G.A., and Pritchett, P.L. 1988, ApJ, 328, 809

Wu, C.S. 1985 Space Sci. Rev., 41, 215

Wu, C.S., and Lee, L.C. 1979 ApJ, 230, 621

Wu, C.S, Tsai, S.T., Xu, M.J., and Shen, J.W. 1981, ApJ, 248, 384

Zlobec, P., and Karlicky, M. 1998, Sol. Phys., 182, 477

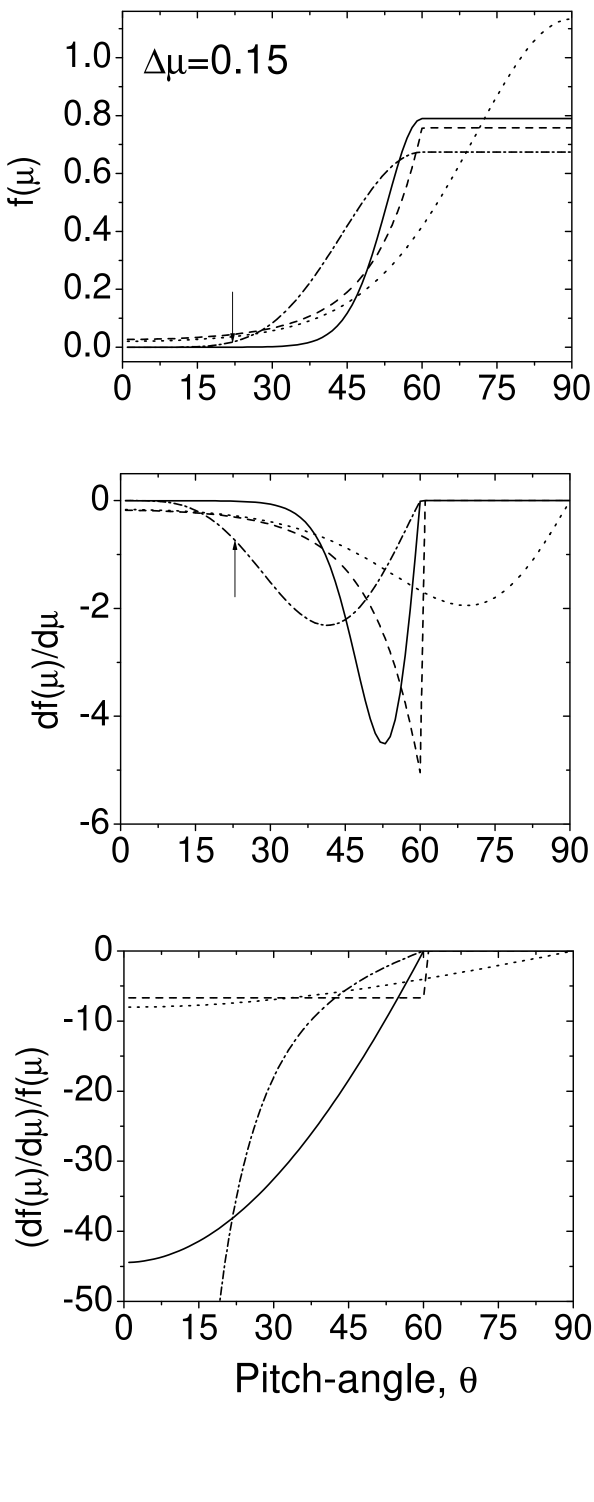

Fig. 1.— Top: Angular distribution functions: gaussian (5), dotted line; sinN loss-cone (6) for $N = 6$, dash-dotted line; exponential loss-cone (7) for $\Delta\mu = 0.15$, dashed line; and gaussian loss-cone (8) for $\Delta\mu = 0.15$, solid line. The distributions are plotted for $\mu_0 = \cos\theta_c = 60^o$, all of them are normalized to unity. Middle: The derivatives of the angular distributions over μ. Bottom: the ratios of the derivatives to the distribution functions.

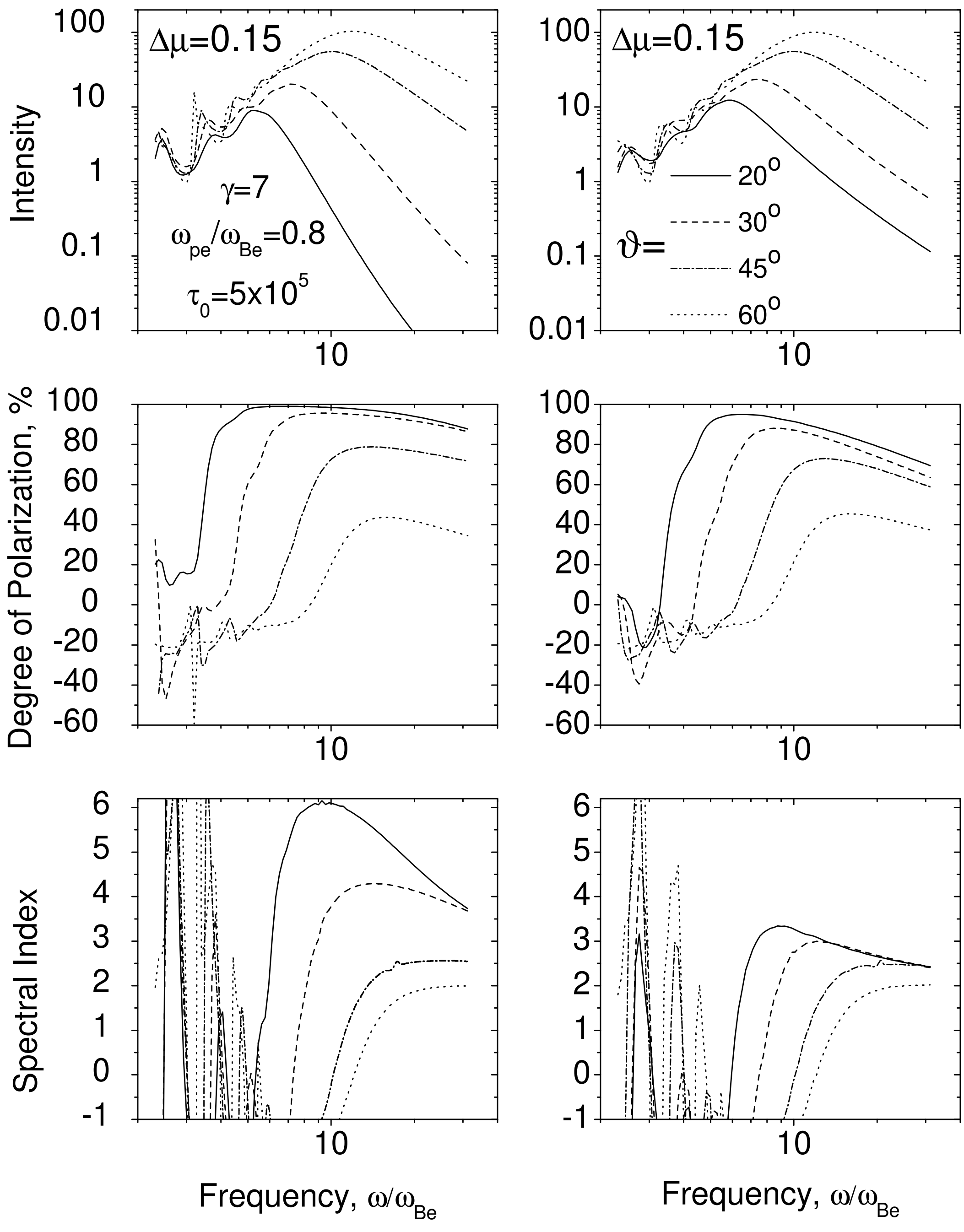

Fig. 2.— Intensity (top), polarization (middle), and spectral index (bottom) of the gyrosynchrotron radio emission produced by fast electrons with the gaussian (left column) and exponential (right column) loss-cone angular distributions calculated for various viewing angles. The parameters are shown in the figure, $\tau_0 \equiv \frac{\pi L \omega_{Be}}{2c} \frac{N_e}{N}$ defines the optical depth of the emission.

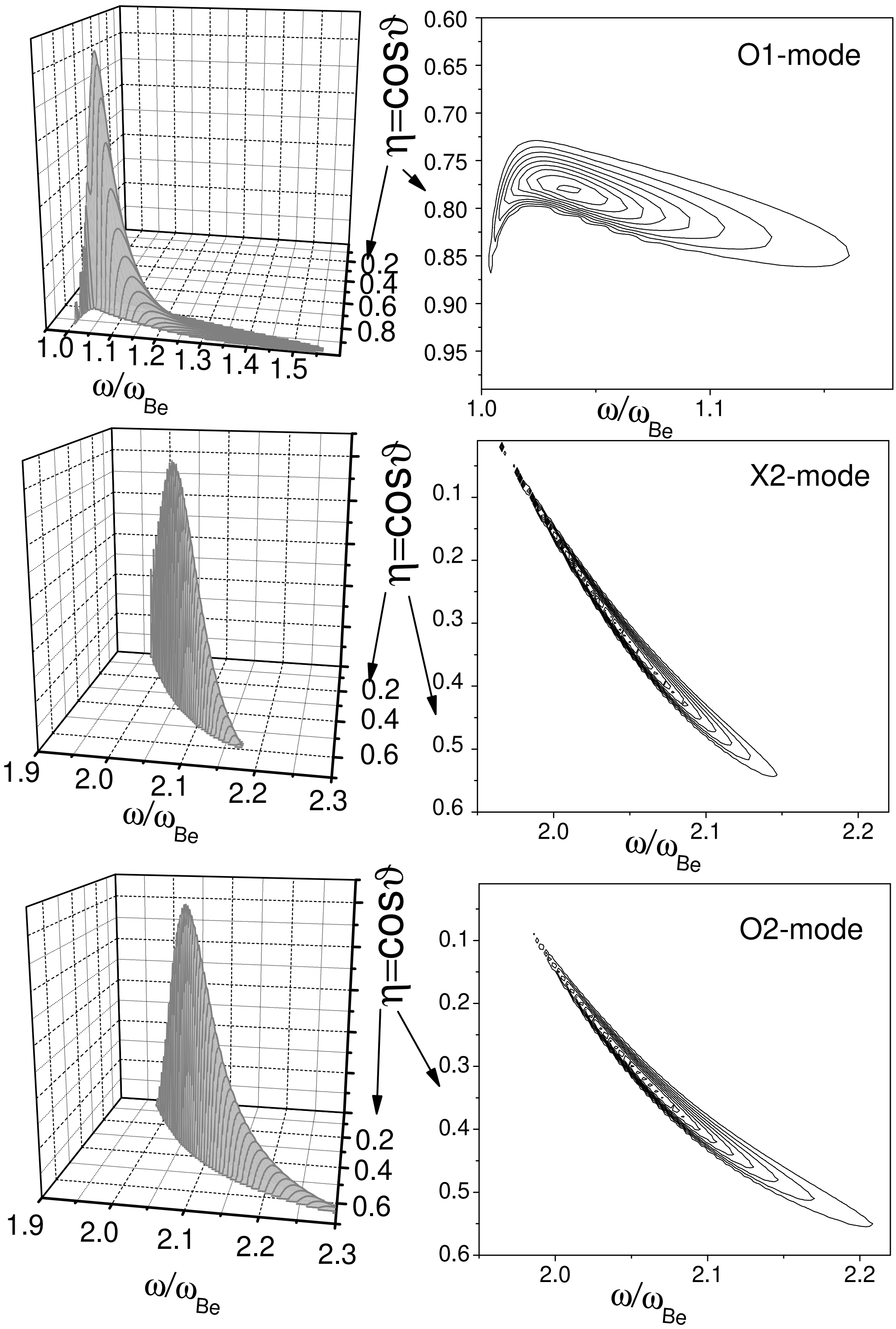

Fig. 3.— 3D- (left column) and contour (right column) plots of the spatial growth rates of O1- (top), X2- (middle), and O2- (bottom) modes for the parameters: $Y = 1$, $\theta_c = 45^o$, $\Delta\mu = 0.15$, $p_0/mc = 0.2$, $p_{br}/mc = 3$, $\gamma = 6$. Note, that the instability region covers a rather broad spectral range, although the spectral bandwidth is small for each selected η value.

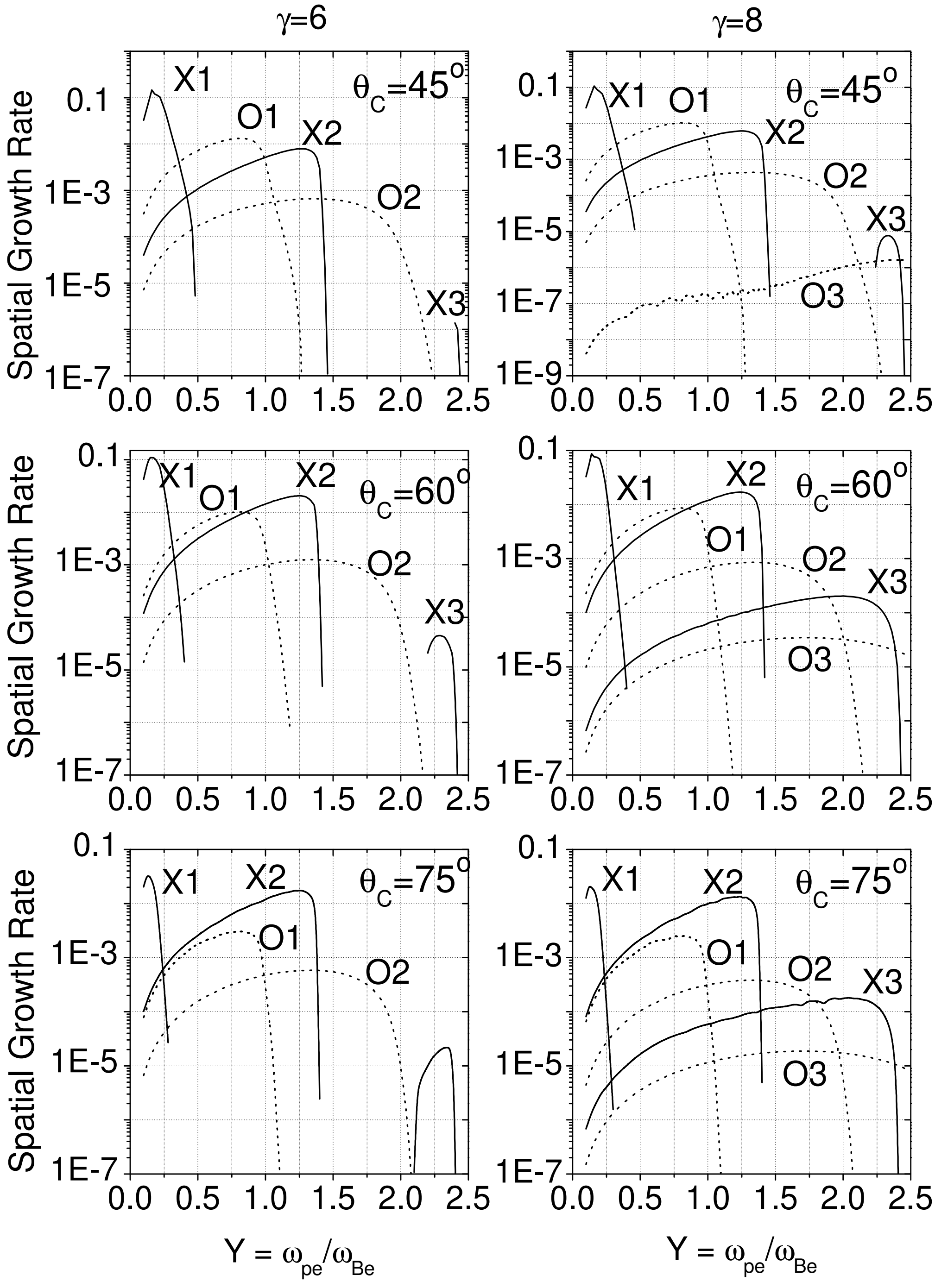

Fig. 4.— Spatial growth rates for three first harmonics of the gyrofrequency for various parameters: $\gamma = 6$ (left column), $\gamma = 8$ (right column); $\theta_c = 45^o$ (top), $\theta_c = 60^o$ (middle), $\theta_c = 75^o$ (bottom). Set of basic parameters is used: $\Delta\mu = 0.15$, $p_0/mc = 0.2$, $p_{br}/mc = 3$.

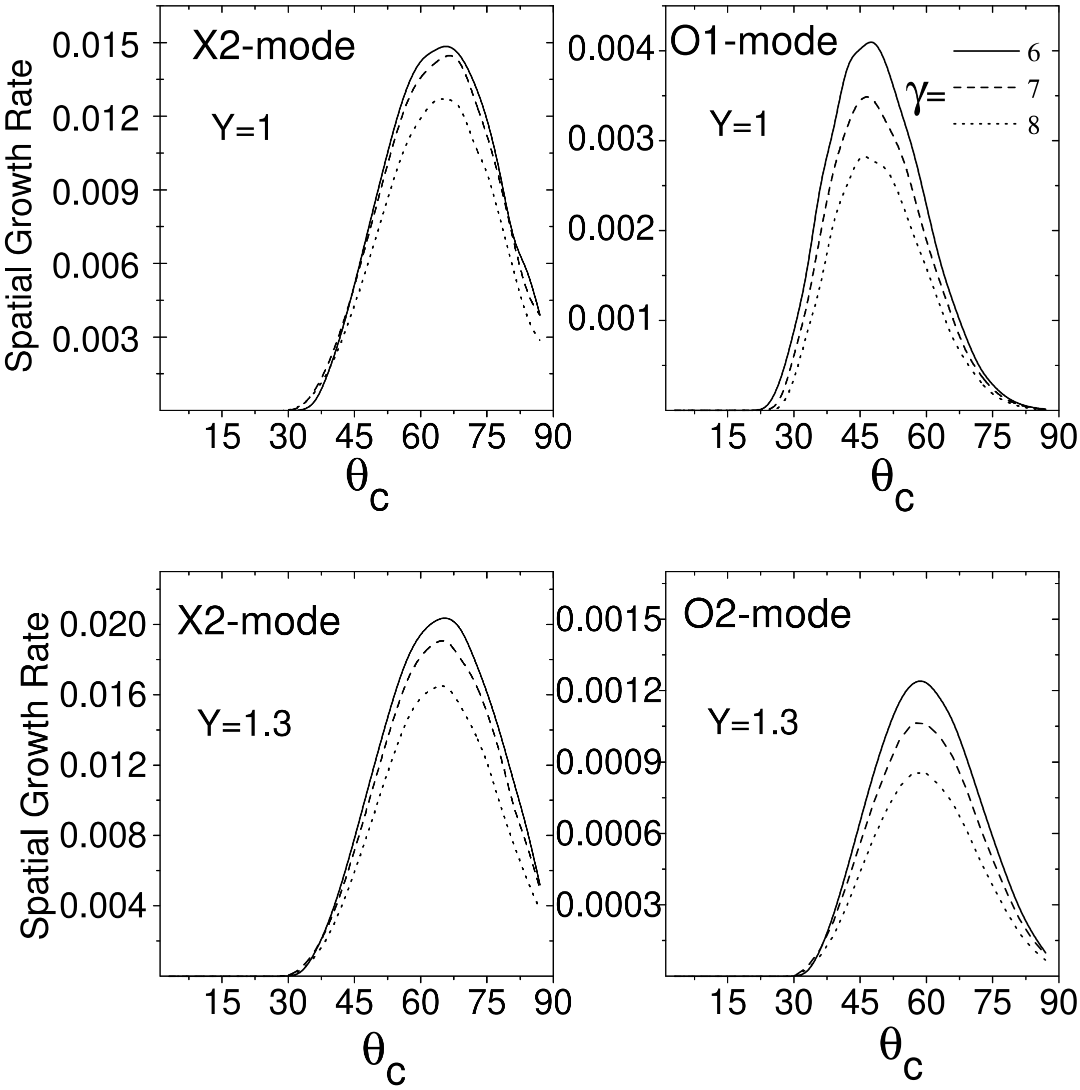

Fig. 5.— Spatial growth rates for X2-, O1-, and O2- modes vs loss-cone angle θ_c for the basic set of parameters and three γ values.

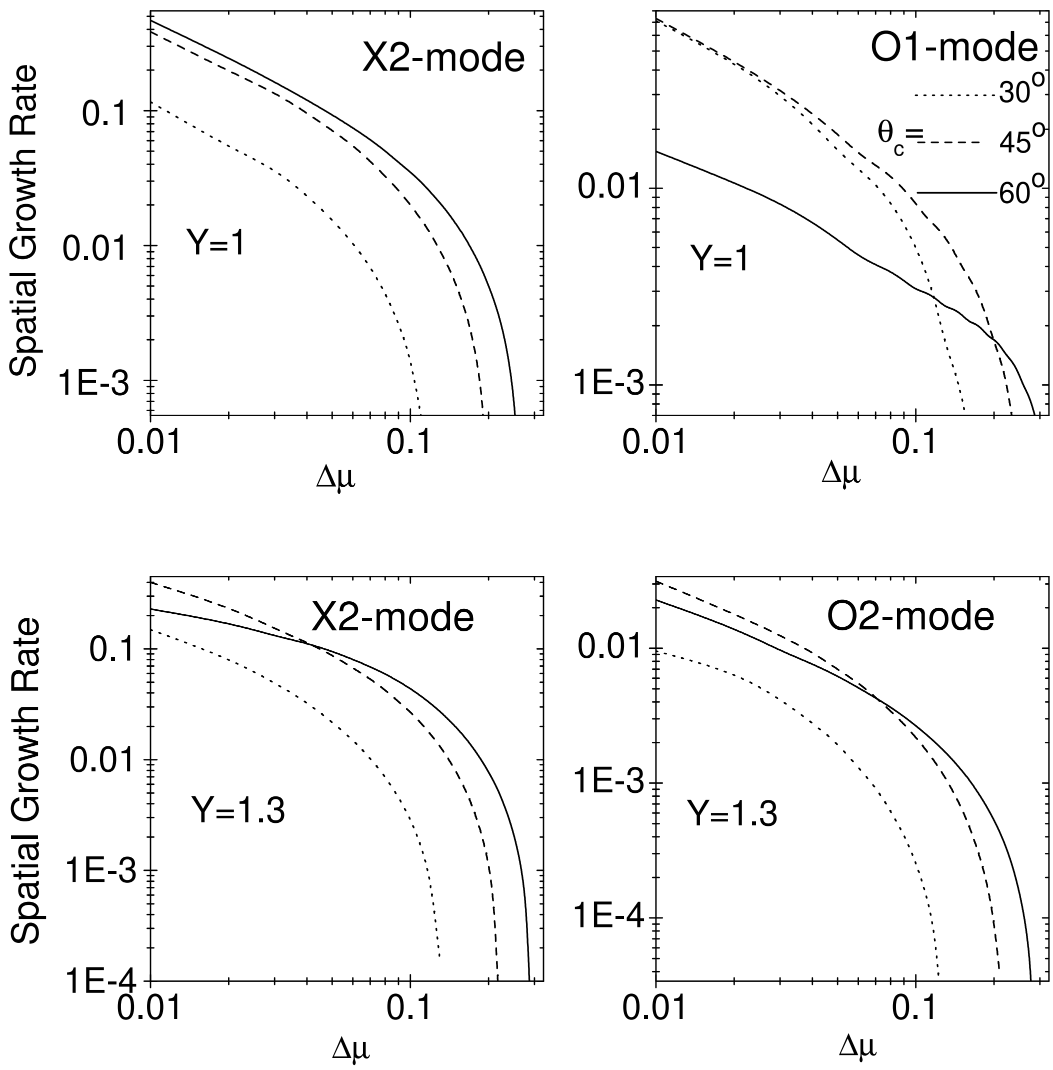

Fig. 6.— Spatial growth rates for X2-, O1-, and O2- modes vs width of the loss-cone distribution $\Delta\mu$ for the basic set of parameters and three θ_c values.

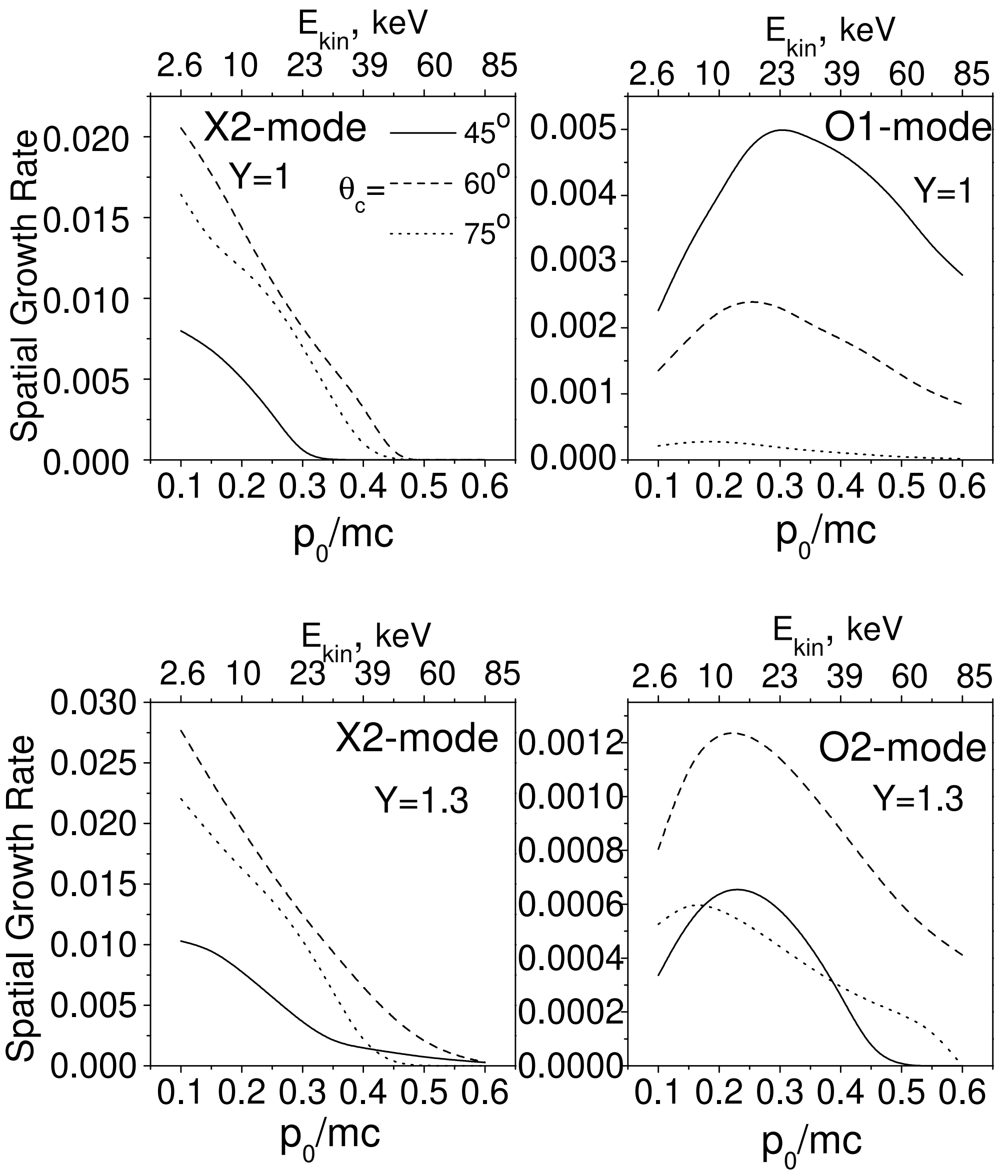

Fig. 7.— Spatial growth rates for X2-, O1-, and O2- modes vs minimal momentum of fast electrons p_0 for the basic set of parameters and three θ_c values.

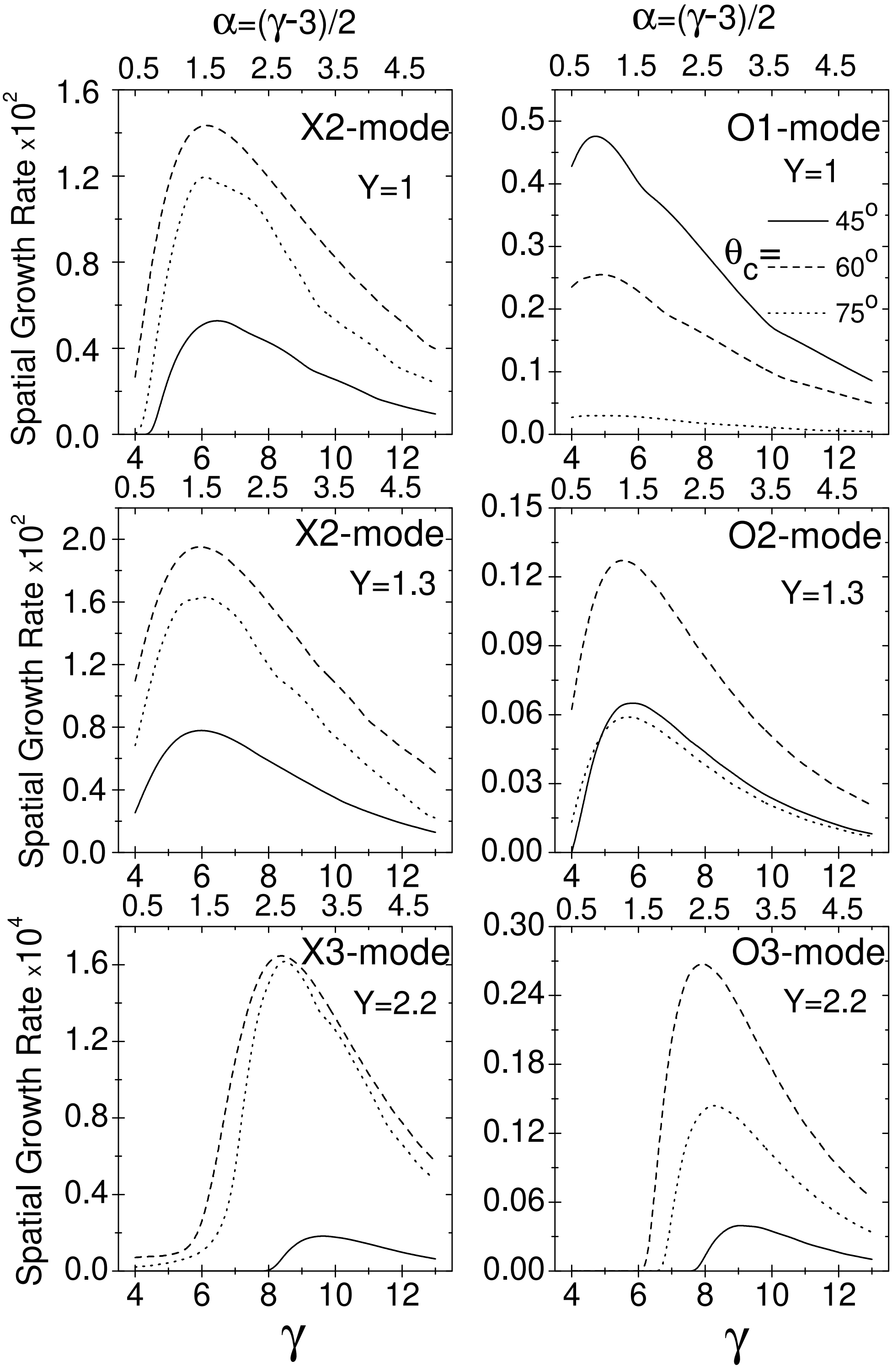

Fig. 8.— Spatial growth rates for X2-, X3-, O1-, O2-, and O3- modes vs spectral index of fast electron distribution γ for the basic set of parameters and three θ_c values.

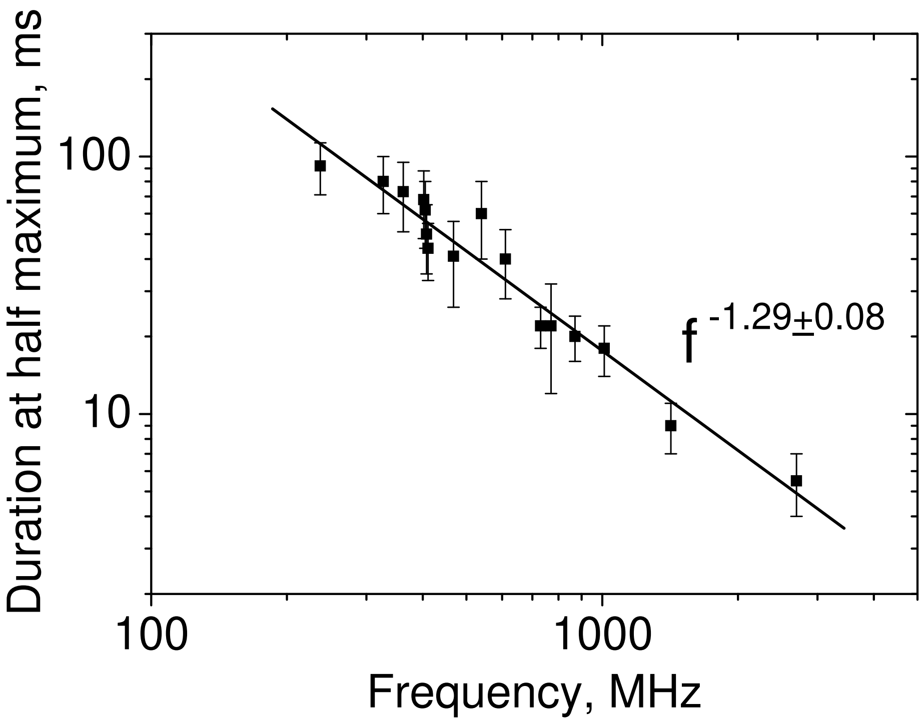

Fig. 9.— Observed duration of spikes at half maximum vs frequency of observation based on published data: 237, 327, 408 and 610 MHz from (Zlobec and Karlicky 1998) and P.Zlobec, private communication, 540 MHz from (Lipatov et al. 2002), 362, 468, 730, 770, 870, 1010 MHz from (Güdel and Benz 1990), and 1420 and 2695 MHz from (Meszarosova et al. 2002). The solid line is the best power-law fit with the index -1.29 ± 0.08.

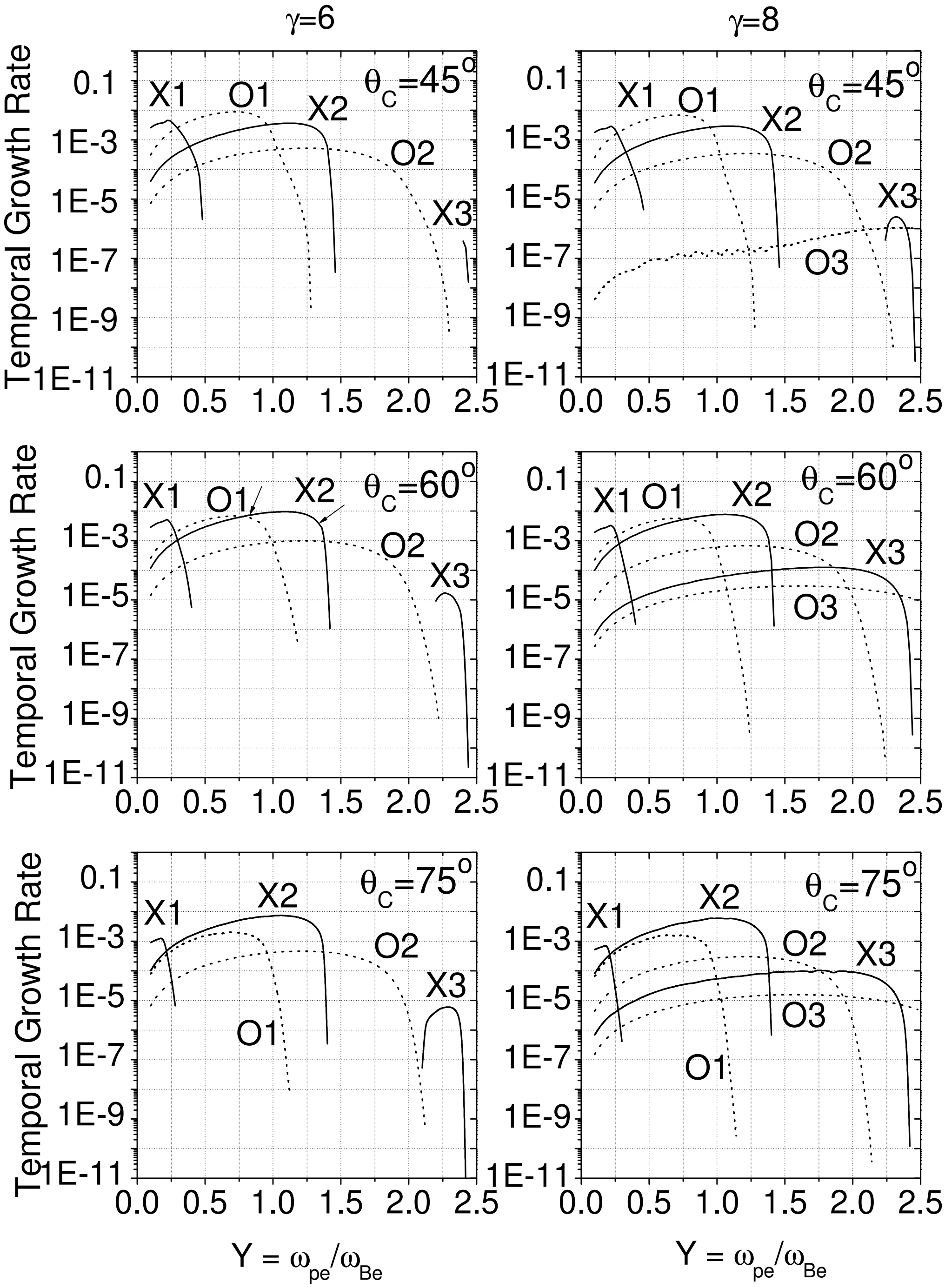

Fig. 10.— Temporal growth rates for three first harmonics of the gyrofrequency for various parameters: $\gamma = 6$ (left column), $\gamma = 8$ (right column); $\theta_c = 45^o$ (top), $\theta_c = 60^o$ (middle), $\theta_c = 75^o$ (bottom). Set of basic parameters is used: $\Delta\mu = 0.15$, $p_0/mc = 0.2$, $p_{br}/mc = 3$.

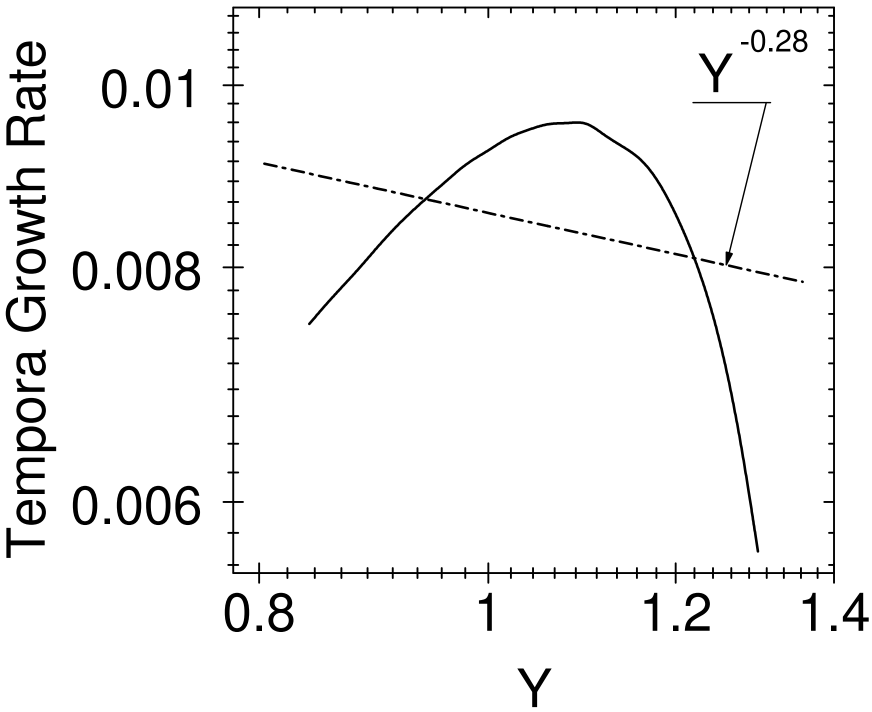

Fig. 11.— A fragment of temporal growth rate curve for X2-mode marked in Fig. 10 by arrows for the parameters: $\gamma = 6$, $\theta_c = 60^o$, $\Delta\mu = 0.15$, $p_0/mc = 0.2$, $p_{br}/mc = 3$. The dot-dashed curve is corresponding linear fit. Although the two curves looks rather differently, the deviation of the true curve from the linear fit is only of the order of or less then 20%.